Highly precision carbon dioxide acoustic wave sensor with minimized humidity interference

Jintao Pang [1], Xianhao Le [1,2], Kai Pang [3], Hanyong Dong [1], Qian Zhang [1], Zhen Xu [3], Chao Gao [3], Yongqing Fu [4], and Jin Xie [1,*]

[1]The State Key Laboratory of Fluid Power and Mechatronic Systems, Zhejiang University, Hangzhou, Zhejiang, People's Republic of China

[2] Department of Electrical and Computer Engineering, National University of Singapore, Singapore

[3] Department of Polymer Science and Engineering, MOE Key Laboratory of Macromolecular Synthesis and Functionalization, Zhejiang University, Hangzhou 310027, People's Republic of China

[4] Faculty of Engineering and Environment, University of Northumbria, Newcastle upon Tyne NE1 8ST, UK

*Corresponding author: Jin Xie (xiejin@zju.edu.cn)

Abstract

Extensive applications of carbon dioxide (CO_2) in various fields, such as food industry, agricultural production, medical and pharmacological industries, have caused a great demand for high-performance CO_2 sensors. However, most existing CO_2 sensors suffer from poor performance in a wet environment and often cannot work accurately in a high humidity condition. In this study, a quartz crystal resonator (QCR) coated with a uniform layer of reduced graphene oxide (RGO) is proposed to detect both the concentrations of CO_2 and water molecules simultaneously, which can be used to significantly minimize the humidity interference. Unlike the other common gas sensors, the RGO-based CO_2 QCR sensor can be operated in different humidity levels and the concentration of CO_2 can be quantified precisely and effectively. Moreover, it has a fast response (~0.4 s), which is also suitable for respiration monitoring. Our results showed that before and after a volunteer did a low-intensity exercise, the sensor could detect the differences of concentrations of CO_2 in the exhaled breath (i.e., 4.50% and 5.15%, respectively).

Keyword: Carbon dioxide sensor, reduced graphene oxide film, humidity influence, human respiration monitoring.

1. Introduction

As one of the key greenhouse gases on earth, carbon dioxide (CO_2) plays an important role in various fields such as manufacture and electronic industries [1], agriculture [2], and medicine [3]. It is critical to develop ultrasensitive CO_2 sensors for these applications and also for health monitoring [4,5]. CO_2 is the product of sufficient oxidation of carbon-containing substances, including the burning of substances and biological respiration. In an organism, oxygen is transported to tissues and cells, and energy-producing oxidization and reactions occur, thus generating CO_2 and water. The exhaled CO_2 can reflect the changes in the metabolism and ventilation systems of a person [6]. Besides, it is also critical to detect CO_2 concentrations for *in situ* monitoring athletic ability [7] and air quality [8].

Several methods have been proposed to detect CO_2 concentration. Normally, nondispersive infrared (NDIR) method possesses the highest resolution for the measurement of CO_2 [9]. However, this method needs expensive and heavy instruments, which are not suitable for real-time, on-site, and continuous monitoring. Therefore some researchers focused on solid-state CO_2 sensors [10] which can enhance sensing performance and reduce size. For instance, graphene has been considered as one of the promising candidates of solid-state sensors for gas sensing due to its planar structure and the large surface-to-volume ratio [11–13]. The mutual attraction between CO_2 molecules and graphene sheet is mainly due to physical adsorption, and the CO_2 molecule acts as an acceptor. Yang *et al.* reported a high-performance CO_2 gas sensor based on graphene using a mechanical cleavage method [14], although this is a low-yield fabrication method. Huang *et al.* developed a CO_2 gas sensor based on reduced graphene oxide (RGO) using a hydrogen plasma [15]. In addition, carboxyl groups that remain on the RGO film can enhance the adsorption capacity of CO_2 [16]. Unfortunately, most of the sensors mentioned above also respond well to water molecules. They normally show a low sensing response in high humidity (sensitivity from 54% to 10% when relative humidity from 37% to 68% in [15]). Therefore, it is critical to find a method to eliminate or minimize the influence of humidity. A promising approach for achieving this purpose is to treat the humidity as a measured object rather than as a disturbance. A commonly reported solution is to use another humidity sensor for calibration [17], but this solution adds extra cost and complexity.

Recently, a new idea has been proposed to distinguish among different gases by using a single sensor (e.g. field-effect transistor sensor or solid-state sensor) to detect multiple responses [18,19]. However, high-performance CO_2 gas sensors which can also detect humidity have not been investigated yet. In this work, we report that using a single gas sensor with various responses we can derive the precise

concentrations of CO_2 and humidity level, simultaneously. As shown in Figure 1, the sensor is based on a quartz crystal resonator (QCR) coated with a uniform RGO layer. By tracking multiple responses, we can determine the concentrations of each gas component after extracting thickness and shear modulus effects of RGO layer on the acoustic loading. We test the sensing performance in a mixture of CO_2 and water molecules at different concentrations, and experimental results show that the concentrations of CO_2 and humidity level can be differentiated and quantified with a high accuracy.

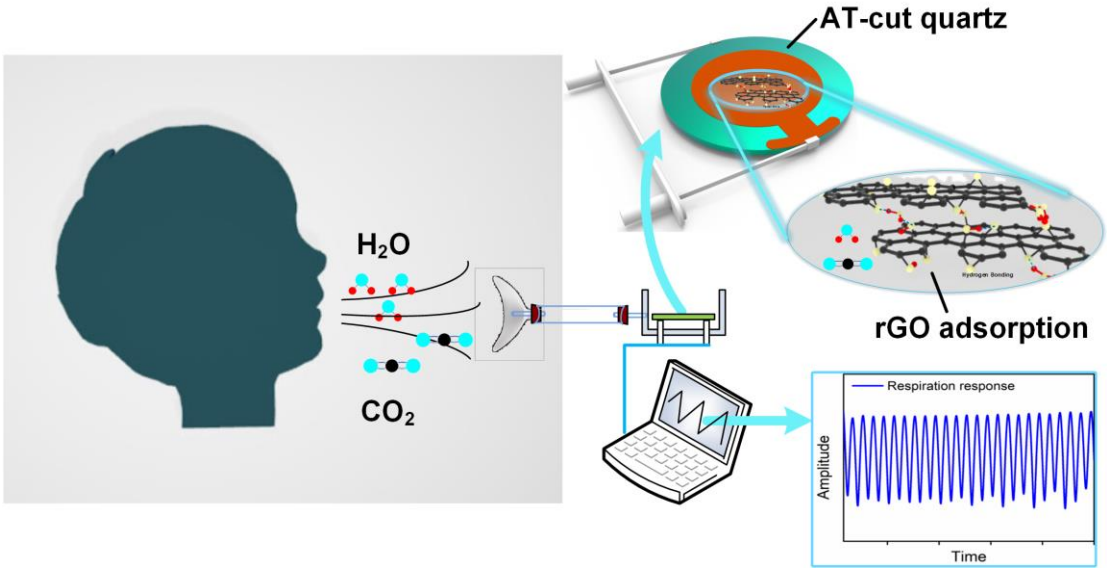

Fig. 1. A schematic drawing of the proposed RGO-based CO_2 sensor. The RGO film was transferred onto the top surface of the AT-cut QCR device. The exhaled gas was detected by the sensor. A LabView program was used to record and analyze the experimental data.

2. Experimental details

2.1 Preparation of RGO-based sensor

The GO sheets were synthesized using the modified Hummers method [20] and then ultrasonically dispersed in water to form GO dispersions with a concentration of 2 mg/ml. By using a vacuum filtration method, the GO dispersions were filtrated through a commercial mixed cellulose ester (MCE) membrane to form GO film. Attributed to the high controllability of vacuum filtration method [21], the obtained filtered GO film shows remarkable uniformity and repeatability. By means of water assistance, the GO film was separated from MCE film and then transferred onto the top surface of a 5 MHz AT-cut QCR device. This was followed by a reduction process of GO film to obtain the RGO film. Here we chose the thermal reduction method to avoid chemical residuals on the RGO surfaces. The GO coated device was heated to 200°C for 2 hours in an oven to remove the oxygen-containing functional groups of GO film,

and the RGO-based gas sensor was then obtained. The 200ºC reduction process can remove most hydroxyl groups but not apparently affect the number of carboxyl groups. The obtained RGO film has lost a lot of hydroxyl groups, which leads to a decreased thickness. Besides, the RGO film has abundant wrinkles and partial functional groups (i.e., carboxyl groups), which are beneficial for CO_2 sensing applications.

A field emission scanning electron microscope (SEM SU-8010) was used to observe the surface morphology of GO and RGO. To characterize the chemical binding of elements and degree of reduction, X-ray photoelectron spectroscopy (XPS) analysis of both GO and RGO was implemented using a Thermo Scientific ESCALAB 250Xi with an X-ray source of Al Ka 1486.6 eV. The calibration was performed using the C peak at 284.8 eV.

2.2 Detection of RGO-based CO_2 and humidity sensor

Pure and dry compressed air was used as the carrier gas to flow through DI water and form humid gas. The dry air, wet air and pure CO_2 were mixed and the mixed gas flowed over the sensor, which was positioned in a testing chamber. By adjusting the mass flow of wet air and CO_2 separately, various concentrations of CO_2 and humidity were modulated using two high-precision controllers and calibrated using a commercial anthracometer (PR-3002LW-CO2WS-N01) and a hygrothermograph (TASI-621), respectively. When exposed to different concentrations of CO_2 and humidity, the admittance data of the sensor were measured using a network analyzer (Agilent E5061B) after a standard calibration. These data were recorded using a LabView program. All the tests were performed at room temperature (20.5℃).

3. Results and discussion

3.1 Film characterization

Figures 2(a) and 2(b) show the SEM images of the GO and RGO films. The GO film is well dispersed and uniform, whereas the RGO film shows wrinkles and defects caused by thermal reduction. To quantify the reduction level and relative amount of each functional group, XPS analysis of both the GO and RGO films was performed. Figure 2(c) shows the C1s spectrum of GO film, which can be deconvoluted into three peaks, including the chemical bonds of C-C at 284.2 eV, C-O at 286.5 eV, and C=O at 288.2 eV. Figure 2(d) shows that the peaks associated with oxygen (i.e., C-O and C=O) of RGO film display decreased intensities when compared with those of the GO. The relative amount of C-O is decreased dramatically, which indicates that the thermal treatment reduced the number of hydroxyl

functional groups effectively. GO film and RGO film have different hydrophilicity and exhibit different water absorption properties. The concentration of oxygen-containing functional groups affects the interaction between water molecules and GO/RGO film. The decreased number of hydroxyl groups leads to a smaller sensitivity to humidity of RGO film [22]. Compared with the GO film, the RGO film has a lower interlayer distance, which also influences the adsorption of water molecules on the film surface [23–25]. Besides, the reduction process leads to wrinkles and there still exist most carboxyl groups in RGO, which are beneficial to CO_2 sensing [16,26].

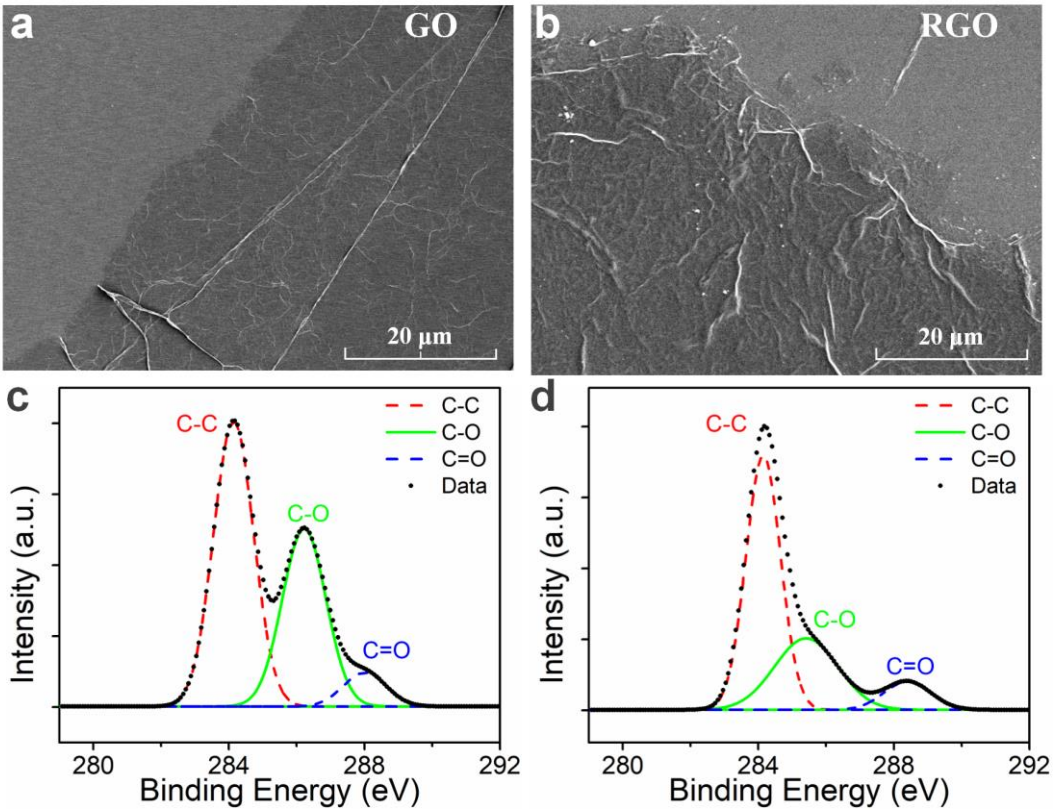

Fig. 2. SEM images of (a) the GO film and (b) the RGO film; The XPS spectrum of (c) the GO film and (d) the RGO film. Compared with GO film, the content of hydroxyl groups of RGO film is decreased significantly.

3.2 CO_2 and humidity sensing

Figure 3 shows the admittance results of the sensor when exposed to CO_2 in different concentrations with different relative humidity levels. As shown in Figures 3(a) and 3(b), the conductance and susceptance of the RGO-based sensors were obtained by varying the CO_2 concentration from 100 to 1000 ppm at room temperature. These data were fitted with an electromechanical model to determine the thickness h and shear modulus G of the coated film. The changes in electrical impedance Z_e caused by coating can be expressed as [27]:

$$Z_e \approx \frac{h}{4k\omega C_0 Z} \cdot \sqrt{G\rho}\tanh(\gamma h) \tag{1}$$

where γ is the complex wave propagation constant, k is the wavenumber, ω is the angular frequency, ρ is the density of the coating film, C_0 and Z are the static capacitance and the complex impedance of quartz. The material constants of quartz in Equation (1) can be obtained from the literature [27] and admittance data of the unloaded device. Then the electrical change Z_e is only related to thickness, shear modulus, and density of the film, and the first two parameters can be fitted by the change of electrical characteristics assuming that the density is constant. The details of numerical calculation can be found in our previous work [28].

The extracted thickness and shear modulus of GO and RGO layers are summarized in Figure 4. As shown in Figure 4(a), the thickness of GO film (empty red circles) is gradually increased from 137.4 to 138.8 nm as the concentration of CO_2 is changed from 100 to 1000 ppm, while the shear modulus of the GO film shows slight fluctuations. The RGO sensor (solid red circles) displays a better sensing response compared to the GO sensor. The thickness increment of RGO film is 2.0 nm after exposure to 1000 ppm of CO_2, which is larger than that of GO film. Furthermore, the shear modulus of RGO film remains unchanged after exposed to CO_2 in different concentrations, which indicates that the adsorption of the CO_2 gas molecules does not affect the interlayer shear modulus of RGO film.

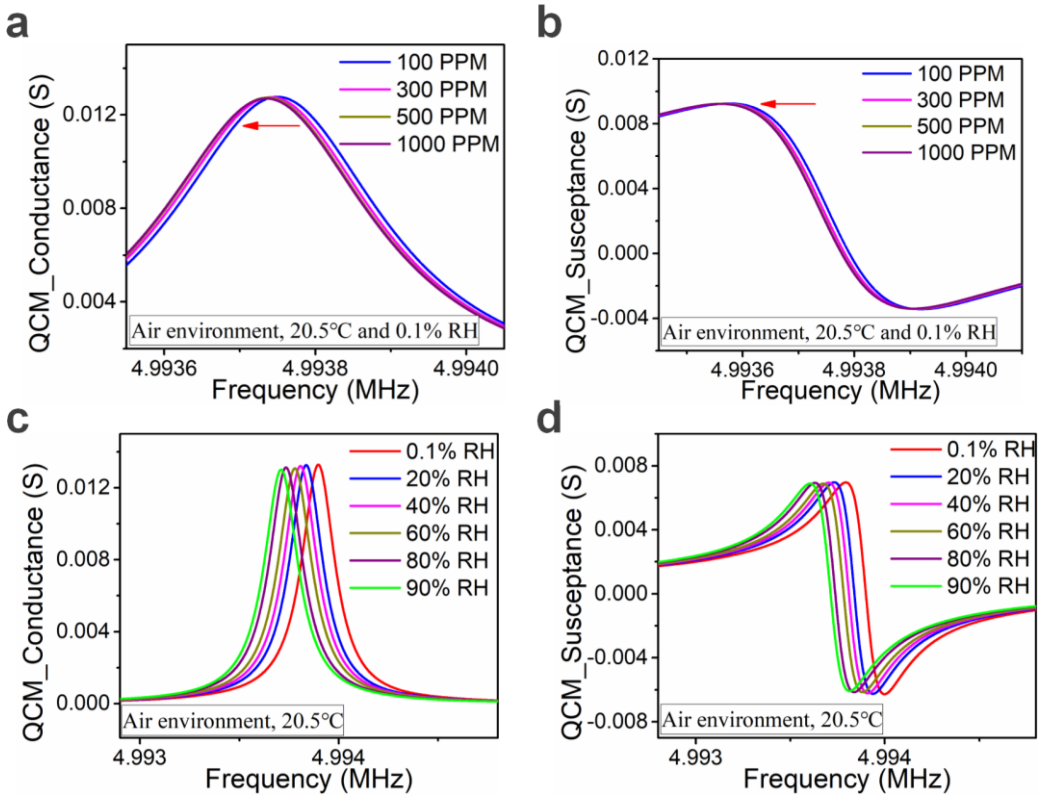

Fig. 3. The measured (a) conductance and (b) susceptance of the RGO-based sensor in different concentrations of CO_2. (c) and (d) indicate the changes of conductance and susceptance of the RGO-based sensor in different humidity.

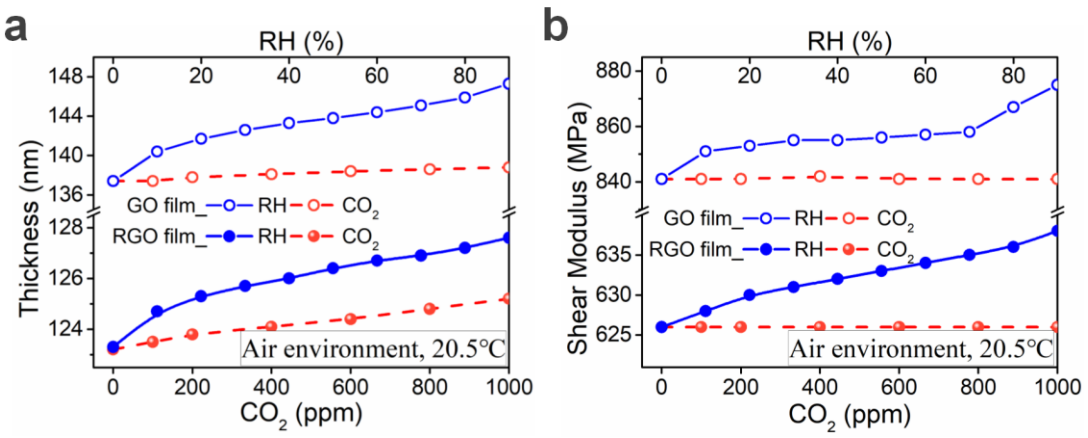

Fig. 4. (a) The effective thickness and (b) shear modulus of the GO (empty circles) and RGO (solid circles) membrane varies with concentrations of CO_2 (red line) and humidity (blue line).

Next, we tested the responses of the RGO sensor at different relative humidity levels, and the results are shown in Figures 3(c) and 3(d). After applying the same extraction method, we obtained the thickness and shear modulus of RGO film as a function of different humidity values from 0.1%RH to 90%RH, as shown in Figures 4(a) and 4(b). Both the thickness and shear modulus are increased with the increase of the relative humidity. The thickness of RGO film (solid blue circles) is increased from 123.2 to 127.6 nm, and the shear modulus of RGO film is increased from 626 to 638 MPa. The thickness of RGO film increases and the shear modulus among the sublayers of RGO is reinforced due to the formation of hydrogen bonding networks [29] between the hydroxyl groups and the permeated moistures [22]. This also demonstrates that there still exist functional groups bonded to the carbon, which is in good agreement with the results from XPS.

The performance of graphene-based CO_2 sensor is greatly affected by humidity [15]. To evaluate the sensing repeatability at different RH levels, we used the mixture of CO_2 and humidity with different concentrations to conduct the experiments. The extracted thickness and shear modulus are shown in Figures 5(a) and (b). At a high relative humidity, the thickness of RGO (shown in Figure 5(a)) increases monotonically with the increase of the concentration of CO_2, but the rate of increase is slightly lower than that in a dry environment. The differences in the responses [15] can be explained by the space occupation of water molecules in a high humidity environment. Some of the space is occupied by water molecules, and the amount of CO_2 gas adsorbed by the RGO film is slightly decreased with the same

increased amount of CO_2 concentration, hence the thickness increment in high humidity level is rather smaller than that in a dry environment.

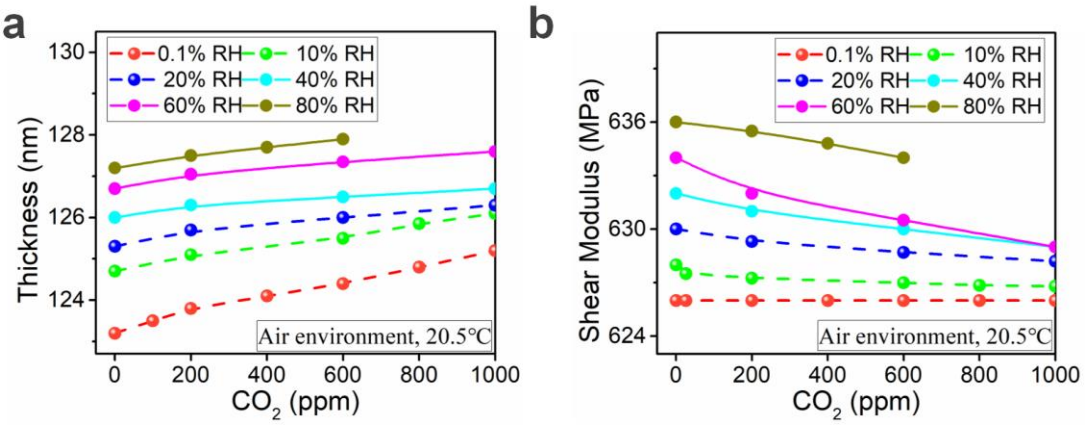

Fig. 5. (a) The thickness and (b) the shear modulus of the RGO film when exposed to the mixture of CO_2 and humidity in different concentrations.

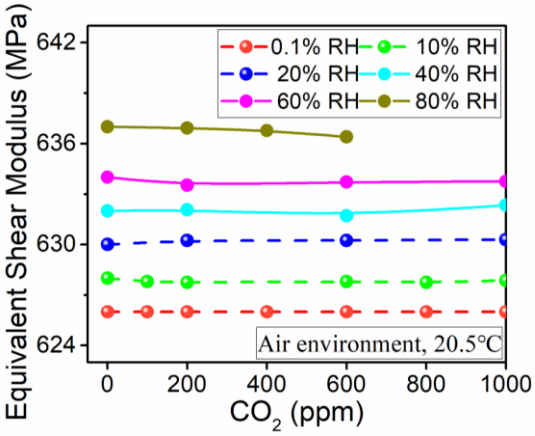

Fig. 6. The equivalent shear modulus caused by the adsorption of CO_2 individually.

Figure 5(b) shows that shear modulus shows significant difference in dry and wet situations. When the humidity level remains unchanged, the shear modulus of RGO film is decreased continuously with the increase of CO_2 concentration. The phenomenon can be attributed to the combined effects of CO_2 and water molecules on shear modulus of RGO film. According to the analysis results shown in Figures 4(a) and 4(b), the adsorption of water molecules enhances the shear modulus of RGO film while CO_2 does not affect its shear modulus. When the RGO sensor is exposed to CO_2 in a wet environment, the CO_2 gas molecules, which replace partial water molecules, reduces the shear resistance and finally reduces the total shear modulus.

To explain the effect of CO_2 adsorption on the shear properties of RGO films, we define the equivalent shear modulus G_{CO2} caused only by CO_2 using the following equation:

$$G_{CO2} = G_0 + \frac{\Delta t \cdot \Delta G - \Delta t_1 \Delta G_1}{\Delta t_{CO2}} \quad (2)$$

where G_0 is the initial shear modulus of RGO film without CO_2 or humidity, $\Delta G_1, \Delta G$ are the changes of shear modulus when exposed to the wet gas and the mixture of CO_2 and humidity. $\Delta t, \Delta t_1, \Delta t_{CO2}$ are the thickness variations caused by the mixture of CO_2 and humidity, by humidity and by CO_2, respectively. Using Equation (2), we calculated the equivalent shear modulus caused by the adsorption of CO_2 individually from the experimental results, and the obtained data are shown in Figure 6. The equivalent shear modulus has no apparent change after exposure to different concentrations of CO_2, which further proves that the adsorption of CO_2 does not affect the shear properties of the RGO film.

These two distinct adsorption mechanisms show the potential to quantify the relative amount of CO_2 and humidity based on the RGO acoustic sensor. According to the original extracted variables, a statistical model about relationships between different gas concentrations and film characteristics was established. The extracted thickness and shear modulus were used as the input variables to specifically identify and quantify the various concentrations of CO_2 and relative humidity. The film properties were measured with 200 ppm, 600 ppm and 1000 ppm CO_2 concentrations in three humidity levels (20%, 40%, and 60% RH). For the reliability testing, we conducted multiple tests every other week for a total of three rounds. The predictive capability of the model was assessed and the obtained results are shown in Figure 7. The classification error is about ~1.5% RH and ~80 ppm CO_2 concentration, as shown in Figure 7(b). In certain applications where the range of CO_2 concentration is large (from 400 ppm to ~4%, for example, monitoring human breath and indoor air quality [30]), the accuracy rate performed by the RGO sensor is satisfactory.

TABLE I COMPARISON OF DIFFERENT PARAMETERS OF VARIOUS CO_2 GAS SENSORS

Sensing film	Type of the device	Temperature (℃)	Range (ppm)	Response	Response time	Reference
Graphene/RGO	Resistance	20~60	10-100	11–26%	~8 s	[14]
	Resistance	23	0-1500	10-54%	4 min	[15]
	Electroluminescent	20	100-1000	5.9%-26.5%	~140 s	[31]
	Resonant	20	100-51500	2%	~0.4 s	This work
MOFs-SnO_2	Chemiresistive	205	500-5000	80.6%	~ 10 s	[32]
Yolk–shell nanospheres	Resistance	100	150-2400	6.3%	2.54 min	[33]
Polypyrrole	Resistance	30	100-950	50%	210 s	[34]
NDIR	optical	25	400-3900	30%	23 s	[35]

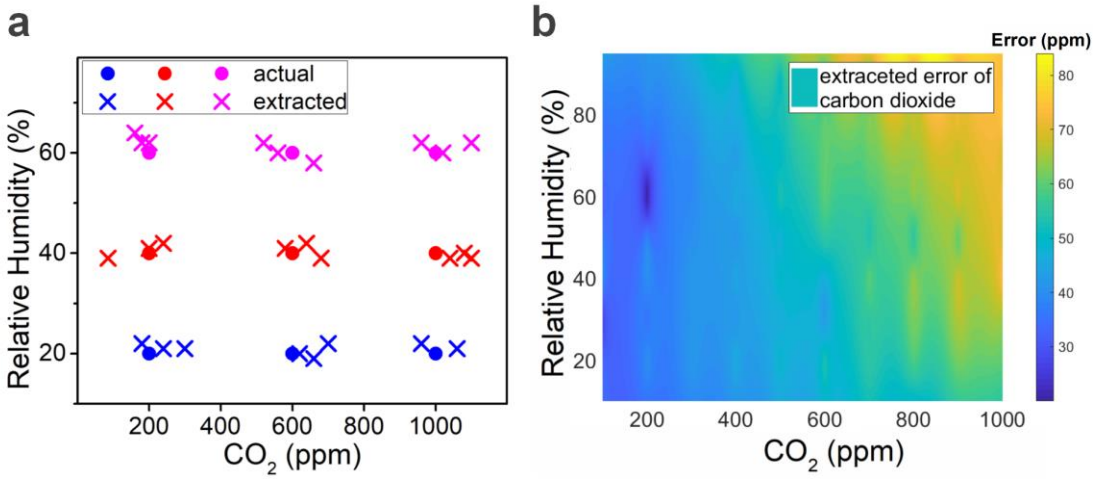

Fig. 7. (a) The comparison between the extracted and actual concentrations of CO_2 and humidity. (b) The color contours of extracted errors in part per million at different concentrations of CO_2 and humidity.

3.3 Respiration detection

The response speed is an important attribute of gas sensors. The response and recovery times were tested, and the results are plotted in Figure 8(a). The response time is defined as the time required for the sensor to reach 90% of the final value after a step change in gas concentrations. According to the curve shown in Figure 8(a), a short response time of 0.2~0.4 s can be obtained, which is far less than those reported in the literature [14,15,31–35]. This fast response promises the possibility of fast analysis applications such as respiration monitoring. Meanwhile, the recovery time is regarded as the time to reach 10% above the initial condition when the target gas is removed from the sensor. The experimental results show that the RGO sensors have a recovery time of ~7 s, which is because the wet and CO_2-containing air surrounding the sensor is diffused slowly and steadily into the atmosphere. This does not

show the real limits of RGO sensor itself. Our results show that the recovery time can be reduced to ~0.6 s when using pure compressed air. In addition, the performance of RGO sensor is compared with those of previously reported CO_2 gas sensor (as listed in Table I). Clearly our newly proposed sensor performs a wide measurement range of CO_2, better than most of the other sensors.

Besides the response speed, thermal stability is also critical for respiration detection. Figure 8(b) exhibits the sensing response of the RGO sensor at different temperatures from 15℃ to 35℃. The temperature of the sensor was accurately measured using a thermocouple probe. As shown in Figure 8(b), the response of RGO sensor at different temperatures shows slight fluctuations, which is much smaller than those responded to CO_2 gas. The excellent thermal stability of RGO sensor is attributed to the nearly zero temperature coefficient of frequency AT-cut quartz.

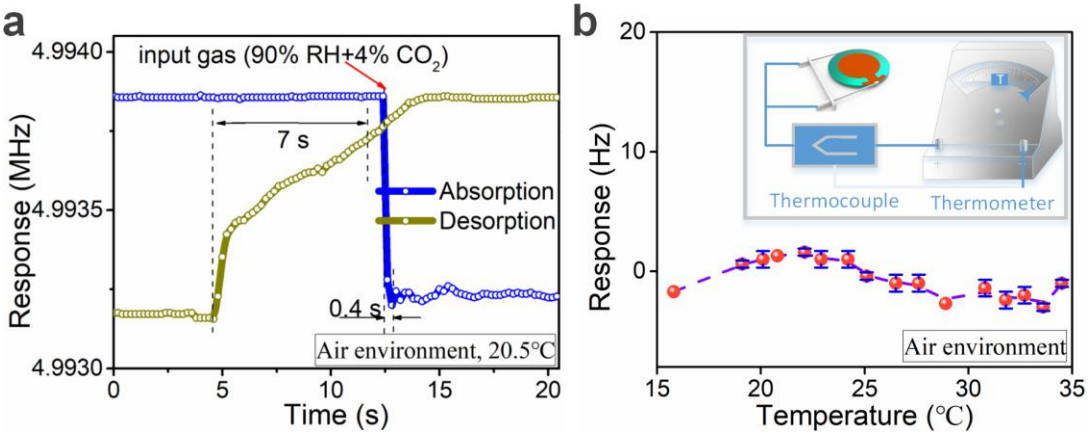

Fig. 8. (a) The response and recovery times of the RGO sensor are 0.2~0.4 s and ~7 s. (b) The sensing responses in different temperature from 15℃ to 35℃.

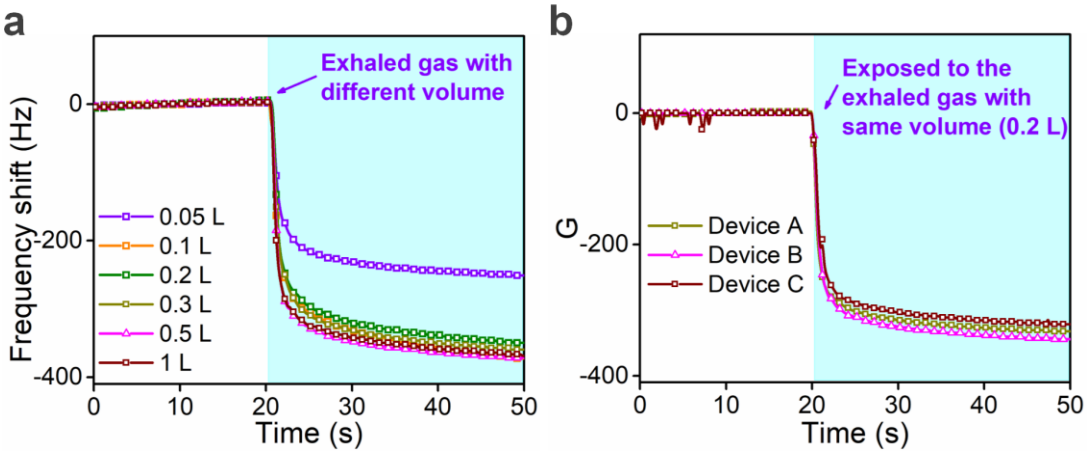

Fig. 9. (a) The frequency response of the RGO sensor when passing exhaled gas with different volume into the test chamber. (b) The sensing performance of the RGO sensors fabricated by the same process.

The repeatability and reproducibility of RGO gas sensor were evaluated before the actual respiration detection. Taking into account the difference in the volume of exhaled gas between individuals, we tested the effect of gas volume on the sensing performance of the RGO sensor. Different volumes (0.05, 0.1, 0.2, 0.3, 0.5 and 1 L) of exhaled gas were collected with gas sample bags. As shown in Figure 9(a), the frequency responses do not have obvious change when the gas volume is greater than 0.1 L. The exhaled volume of a normal adult at rest is about 0.4 ~ 0.6 L, meaning that the volume of exhaled gas does not affect the test results in most cases.

To analyze the influence of the degree of coating film on sensing performance, three RGO sensors (Device A, B, and C) were fabricated and tested in the same batch. Device A, B, and C consist of the same quartz crystal resonator and the RGO film. Attributed to uniformity of sensing films produced by vacuum filtration method, thickness difference of these films is less than several nanometers. However, the sensing film area of each device will be slightly different due to the manual transfer process. Here we made the area of the film slightly larger than the area of the electrode. This is because the energy of the resonator is concentrated in the electrode region, and the sensing film outside the electrode does not affect the resonant state. As shown in Figure 9(b), there is almost no difference in the response of these sensors when exposed to the exhaled gas. These test results exhibit that the proposed sensors have good repeatability and reproducibility in terms of volume of exhaled gas and degree of cover by sensing films.

The fast response speed, good stability and excellent repeatability make the RGO sensor suitable for human respiration detection. Different respiratory rates and metabolic conditions of different persons lead to different components in the exhaled gas. Here we set up two groups of exhalations: (1) normal breath before exercise (BE); and (2) deep breath after exercise (AE). Typical results of different responses of these two groups are depicted in Figure 10. The corresponding concentrations of CO_2 and relative humidity are extracted and also shown in the figure. It can be observed that the signal responds rapidly to the exhaled gas, which is due to the change of gas composition. By comparing Figures 10(a) and 10(b), we can find that the concentrations of moisture and CO_2 in the exhaled gas are increased significantly after a low-intensity exercise (from 4.50% to 5.15%), whose number is in good agreements with those from healthy individuals [36]. In addition, the exhaled gas of AE has a higher humidity level than that of BE. These results indicate that the RGO sensor can be potentially used in human respiration monitoring and body metabolism detection.

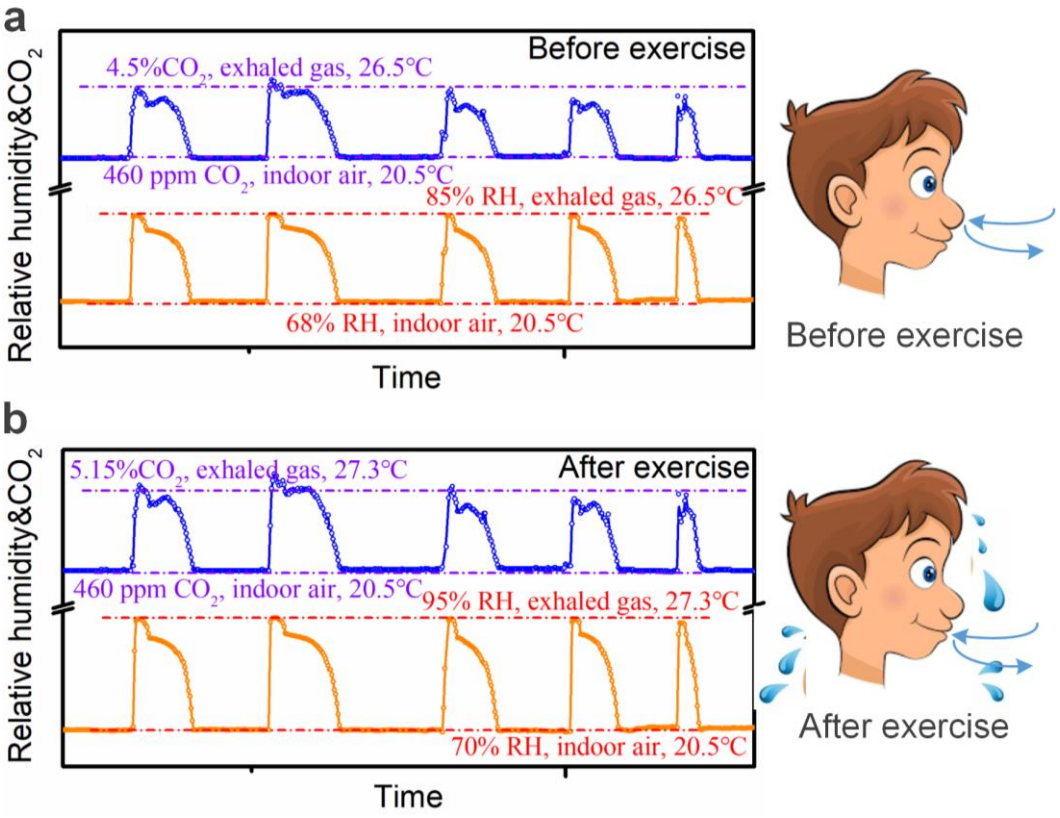

Fig. 10. (a) and (b) depict the extracted concentrations of CO_2 and humidity when exposed to the human expiration before and after a low-intensity exercise.

4. Conclusions

In this work, we have developed the models to extract the thickness and shear modulus of the RGO film exposed to CO_2 and humidity at different concentrations. According to these results, the RGO films have different mechanisms for adsorbing CO_2 and water molecules. Using this phenomenon, we propose a virtual RGO-based gas sensor to simultaneously identify and quantify the concentrations of CO_2 and relative humidity. This RGO sensor has fast response speed, good stability and excellent repeatability. The measurement error is within 1.5% RH and 80 ppm CO_2 concentration. Moreover, the fast response time (0.2~0.4 s) shows potential applications using the acoustic sensor for human expiration monitoring. By analyzing the response signals, we can easily obtain the composition of exhaled gas and reflect the metabolic states of the human body.

Acknowledgments

This work is supported by the “National Natural Science Foundation of China (51875521)”, the “Zhejiang Provincial Natural Science Foundation of China (LZ19E050002)”, the “Science Fund for

Creative Research Groups of National Natural Science Foundation of China (51821093)", and the Engineering Physics and Science Research Council of UK (EPSRC EP/P018998/1). The author J. Pang acknowledges support from the program of China Scholarship Council (No. 202006320274) and 2020 Zhejiang University Academic Award for Outstanding Doctoral Candidates (No.202017).

References

[1] A.M. Parvez, M.T. Afzal, T.G. Victor Hebb, M. Schmid, Utilization of CO2 in thermochemical conversion of biomass for enhanced product properties: A review, J. CO2 Util. 40 (2020) 101217. doi:https://doi.org/10.1016/j.jcou.2020.101217.

[2] S. Neethirajan, D.S. Jayas, S. Sadistap, Carbon Dioxide (CO2) Sensors for the Agri-food Industry—A Review, Food Bioprocess Technol. 2 (2009) 115–121. doi:10.1007/s11947-008-0154-y.

[3] C. Cinquemani, C. Boyle, E. Bach, E. Schollmeyer, Inactivation of microbes using compressed carbon dioxide—An environmentally sound disinfection process for medical fabrics, J. Supercrit. Fluids. 42 (2007) 392–397. doi:https://doi.org/10.1016/j.supflu.2006.11.001.

[4] X. Zhang, P. Wargocki, Z. Lian, C. Thyregod, Effects of exposure to carbon dioxide and bioeffluents on perceived air quality, self-assessed acute health symptoms, and cognitive performance, Indoor Air. 27 (2017) 47–64. doi:10.1111/ina.12284.

[5] C. Zhu, K. Kobayashi, I. Loladze, J. Zhu, Q. Jiang, X. Xu, G. Liu, S. Seneweera, K.L. Ebi, A. Drewnowski, N.K. Fukagawa, L.H. Ziska, Carbon dioxide (CO2) levels this century will alter the protein, micronutrients, and vitamin content of rice grains with potential health consequences for the poorest rice-dependent countries, Sci. Adv. 4 (2018) eaaq1012. doi:10.1126/sciadv.aaq1012.

[6] F. Xu, J. Uh, M.R. Brier, J. Hart, U.S. Yezhuvath, H. Gu, Y. Yang, H. Lu, The Influence of Carbon Dioxide on Brain Activity and Metabolism in Conscious Humans, J. Cereb. Blood Flow Metab. 31 (2010) 58–67. doi:10.1038/jcbfm.2010.153.

[7] R. Arena, M. Guazzi, J. Myers, Prognostic value of end-tidal carbon dioxide during exercise testing in heart failure, Int. J. Cardiol. 117 (2007) 103–108. doi:10.1016/j.ijcard.2006.04.058.

[8] K. Kaneyasu, K. Otsuka, Y. Setoguchi, S. Sonoda, T. Nakahara, I. Aso, N. Nakagaichi, A carbon dioxide gas sensor based on solid electrolyte for air quality control, Sensors Actuators B Chem. 66 (2000) 56–58. doi:https://doi.org/10.1016/S0925-4005(99)00411-6.

[9] J. Hodgkinson, R. Smith, W.O. Ho, J.R. Saffell, R.P. Tatam, Non-dispersive infra-red (NDIR) measurement of carbon dioxide at 4.2μm in a compact and optically efficient sensor, Sensors Actuators B Chem. 186 (2013) 580–588. doi:https://doi.org/10.1016/j.snb.2013.06.006.

[10] J. Tang, D.D. Baldocchi, Y. Qi, L. Xu, Assessing soil CO2 efflux using continuous measurements of CO2 profiles in soils with small solid-state sensors, Agric. For. Meteorol. 118 (2003) 207–220. doi:https://doi.org/10.1016/S0168-1923(03)00112-6.

[11] S. Basu, P. Bhattacharyya, Recent developments on graphene and graphene oxide based solid state gas sensors, Sensors Actuators B Chem. 173 (2012) 1–21. doi:https://doi.org/10.1016/j.snb.2012.07.092.

[12] H. Grajek, J. Jonik, Z. Witkiewicz, T. Wawer, M. Purchała, Applications of Graphene and Its Derivatives in Chemical Analysis, Crit. Rev. Anal. Chem. 50 (2020) 445–471. doi:10.1080/10408347.2019.1653165.

[13] J.D. Fowler, M.J. Allen, V.C. Tung, Y. Yang, R.B. Kaner, B.H. Weiller, Practical Chemical Sensors from Chemically Derived Graphene, ACS Nano. 3 (2009) 301–306. doi:10.1021/nn800593m.

[14] H.J. Yoon, D.H. Jun, J.H. Yang, Z. Zhou, S.S. Yang, M.M.-C. Cheng, Carbon dioxide gas sensor using a graphene sheet, Sensors Actuators B Chem. 157 (2011) 310–313. doi:https://doi.org/10.1016/j.snb.2011.03.035.

[15] S. Muhammad Hafiz, R. Ritikos, T.J. Whitcher, N. Md. Razib, D.C.S. Bien, N. Chanlek, H. Nakajima, T. Saisopa, P. Songsiriritthigul, N.M. Huang, S.A. Rahman, A practical carbon dioxide gas sensor using room-temperature hydrogen plasma reduced graphene oxide, Sensors Actuators B Chem. 193 (2014) 692–700. doi:https://doi.org/10.1016/j.snb.2013.12.017.

[16] R. Dawson, D.J. Adams, A.I. Cooper, Chemical tuning of CO2 sorption in robust nanoporous organic polymers, Chem. Sci. 2 (2011) 1173–1177. doi:10.1039/C1SC00100K.

[17] A. Rehman, A. Hamilton, A. Chung, G.A. Baker, Z. Wang, X. Zeng, Differential Solute Gas Response in Ionic-Liquid-Based QCM Arrays: Elucidating Design Factors Responsible for

Discriminative Explosive Gas Sensing, Anal. Chem. 83 (2011) 7823–7833. doi:10.1021/ac201583c.

[18] P. Reimann, A. Schütze, Sensor Arrays, Virtual Multisensors, Data Fusion, and Gas Sensor Data Evaluation BT - Gas Sensing Fundamentals, in: C.-D. Kohl, T. Wagner (Eds.), Springer Berlin Heidelberg, Berlin, Heidelberg, 2014: pp. 67–107. doi:10.1007/5346_2013_52.

[19] Z. Ankara, T. Kammerer, A. Gramm, A. Schütze, Low power virtual sensor array based on a micromachined gas sensor for fast discrimination between H2, CO and relative humidity, Sensors Actuators B Chem. 100 (2004) 240–245. doi:https://doi.org/10.1016/j.snb.2003.12.072.

[20] W.S. Hummers, R.E. Offeman, Preparation of Graphitic Oxide, J. Am. Chem. Soc. 80 (1958) 1339–1339. doi:10.1021/ja01539a017.

[21] Z. Wu, Transparent, Conductive Carbon Nanotube Films, Science (80-.). 305 (2004) 1273–1276. doi:10.1126/science.1101243.

[22] R.A. Soler-Crespo, W. Gao, L. Mao, H.T. Nguyen, M.R. Roenbeck, J.T. Paci, J. Huang, S.T. Nguyen, H.D. Espinosa, The Role of Water in Mediating Interfacial Adhesion and Shear Strength in Graphene Oxide, ACS Nano. 12 (2018) 6089–6099. doi:10.1021/acsnano.8b02373.

[23] N. Song, X. Gao, Z. Ma, X. Wang, Y. Wei, C. Gao, A review of graphene-based separation membrane: Materials, characteristics, preparation and applications, Desalination. 437 (2018) 59–72. doi:https://doi.org/10.1016/j.desal.2018.02.024.

[24] A. V Talyzin, T. Hausmaninger, S. You, T. Szabó, The structure of graphene oxide membranes in liquid water, ethanol and water–ethanol mixtures, Nanoscale. 6 (2014) 272–281. doi:10.1039/C3NR04631A.

[25] D.I. Petukhov, E.A. Chernova, O.O. Kapitanova, O. V Boytsova, R.G. Valeev, A.P. Chumakov, O. V Konovalov, A.A. Eliseev, Thin graphene oxide membranes for gas dehumidification, J. Memb. Sci. 577 (2019) 184–194. doi:https://doi.org/10.1016/j.memsci.2019.01.041.

[26] J. Nishino, Adsorption of water vapor and carbon dioxide at carboxylic functional groups on the surface of coal, Fuel. 80 (2001) 757–764. doi:https://doi.org/10.1016/S0016-2361(00)00136-8.

[27] R. Lucklum, C. Behling, R.W. Cernosek, S.J. Martin, Determination of complex shear modulus with thickness shear mode resonators, J. Phys. D. Appl. Phys. 30 (1997) 346–356. doi:10.1088/0022-3727/30/3/006.

[28] J. Pang, X. Le, Q. Zhang, C. Wu, J. Xie, The Shear Modulus Determination via Quartz Crystal Resonator for Graphene Oxide Film Prepared by Drop Casting, in: 2020 IEEE 33rd Int. Conf. Micro Electro Mech. Syst., 2020: pp. 830–833. doi:10.1109/MEMS46641.2020.9056303.

[29] M. Daly, C. Cao, H. Sun, Y. Sun, T. Filleter, C.V. Singh, Interfacial Shear Strength of Multilayer Graphene Oxide Films, ACS Nano. 10 (2016) 1939–1947. doi:10.1021/acsnano.5b05771.

[30] M. Leidinger, T. Sauerwald, W. Reimringer, G. Ventura, A. Schütze, Selective detection of hazardous VOCs for indoor air quality applications using a virtual gas sensor array, J. Sensors Sens. Syst. 3 (2014) 253–263. doi:10.5194/jsss-3-253-2014.

[31] Y. Seekaew, C. Wongchoosuk, A novel graphene-based electroluminescent gas sensor for carbon dioxide detection, Appl. Surf. Sci. 479 (2019) 525–531. doi:https://doi.org/10.1016/j.apsusc.2019.02.100.

[32] M.E. DMello, N.G. Sundaram, S.B. Kalidindi, Assembly of ZIF-67 Metal–Organic Framework over Tin Oxide Nanoparticles for Synergistic Chemiresistive CO2 Gas Sensing, Chem. – A Eur. J. 24 (2018) 9220–9223. doi:https://doi.org/10.1002/chem.201800847.

[33] C.A. Zito, T.M. Perfecto, A.-C. Dippel, D.P. Volanti, D. Koziej, Low-Temperature Carbon Dioxide Gas Sensor Based on Yolk–Shell Ceria Nanospheres, ACS Appl. Mater. Interfaces. 12 (2020) 17745–17751. doi:10.1021/acsami.0c01641.

[34] S.A. Waghuley, S.M. Yenorkar, S.S. Yawale, S.P. Yawale, Application of chemically synthesized conducting polymer-polypyrrole as a carbon dioxide gas sensor, Sensors Actuators B Chem. 128 (2008) 366–373. doi:https://doi.org/10.1016/j.snb.2007.06.023.

[35] L. Scholz, A.O. Perez, B. Bierer, P. Eaksen, J. Wöllenstein, S. Palzer, Carbon dioxide sensor for mobile devices: A novel approach for low-power consuming, highly sensitive NDIR sensors, in: 2016 IEEE SENSORS, 2016: pp. 1–3. doi:10.1109/ICSENS.2016.7808788.

[36] V.G. Ageev, O.Y. Nikiforova, Optoacoustic Determination of Carbon Dioxide Concentration in Exhaled Breath in Various Human Diseases*, J. Appl. Spectrosc. 83 (2016) 820–825. doi:10.1007/s10812-016-0369-z.